

Multifunctional Coaxial Energy Fiber toward Energy Harvesting, Storage, and Utilization

Jing Han,[▽] Chongyang Xu,[▽] Jintao Zhang, Nuo Xu, Yao Xiong, Xiaole Cao, Yuchen Liang, Li Zheng, Jia Sun, Junyi Zhai,* Qijun Sun,* and Zhong Lin Wang*



Cite This: *ACS Nano* 2021, 15, 1597–1607



Read Online

ACCESS |

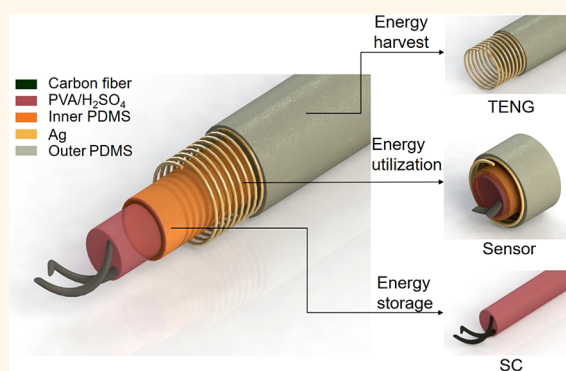
Metrics & More

Article Recommendations

Supporting Information

ABSTRACT: Fibrous energy–autonomy electronics are highly desired for wearable soft electronics, human–machine interfaces, and the Internet of Things. How to effectively integrate various functional energy fibers into them and realize versatile applications is an urgent need to be fulfilled. Here, a multifunctional coaxial energy fiber has been developed toward energy harvesting, energy storage, and energy utilization. The energy fiber is composed of an all fiber-shaped triboelectric nanogenerator (TENG), supercapacitor (SC), and pressure sensor in a coaxial geometry. The inner core is a fibrous SC by a green activation strategy for energy storage; the outer sheath is a fibrous TENG in single-electrode mode for energy harvesting, and the outer friction layer and inner layer (covered with Ag) constitute a self-powered pressure sensor. The electrical performances of each energy component are systematically investigated. The fibrous SC shows a length specific capacitance density of $13.42 \text{ mF}\cdot\text{cm}^{-1}$, good charging/discharging rate capability, and excellent cycling stability ($\sim 96.6\%$ retention). The fibrous TENG shows a maximum power of $2.5 \mu\text{W}$ to power an electronic watch and temperature sensor. The pressure sensor has a good enough sensitivity of $1.003 \text{ V}\cdot\text{kPa}^{-1}$ to readily monitor the real-time finger motions and work as a tactile interface. The demonstrated energy fibers have exhibited stable electrochemical and mechanical performances under mechanical deformation, which make them attractive for wearable electronics. The demonstrated soft and multifunctional coaxial energy fiber is also of great significance in a sustainable human–machine interactive system, intelligent robotic skin, security tactile switches, *etc.*

KEYWORDS: energy fiber, multifunctional, coaxial, nanogenerator, self-powered system



Wearable soft electronics, intelligent medical devices, big data, and the connection nodes of the Internet of Things call for sustainable and self-powered multifunctional electronic devices and sensors.^{1–5} Versatile and sophisticated energy autonomous electronics are highly desired to escape from the short lifetime, requirements of replacement/maintenance, inevitable pollution, and even potential explosive problems during the huge amount of usage of batteries. Harvesting the surrounding and distributed energy to store or directly use in a self-powered system is an efficient route to solving the above problems.^{6,7} Available options for energy autonomy generally comprise of energy harvesting components,⁸ energy storage units,^{9,10} and relevant electrical appliances/sensors/actuators,^{11,12} which have struggled to be pursued by developing a self-charging energy package,¹³ constructing hybrid nanogenerators,¹⁴ pairing power management circuits,^{15,16} formulating standards/figures-of-merit,¹⁷ and innovating energy-harvesting strategies (e.g., tribovoltaic effect¹⁸ and dielectric breakdown effects^{19,20}). Considering that the intrinsic human motions/actions are commonly in low

frequency ($< 5 \text{ Hz}$), a triboelectric nanogenerator (TENG)²¹ with output power proportion to the action frequency ($P_{\text{out}} \propto f$) is more beneficial to be adopted to harvest the low-frequency and irregular mechanical energy.²² For energy storage units, supercapacitors (SCs) capable of being assembled with excellent flexibility, broad structure design space, high rate capacity, and long-term stability are optimal choices for wearable power sources in daily life.^{23–29} Thus, the fabricated energy package can be sustainably and readily used to power portable electronics,³⁰ work as pressure/strain sensors,³¹ interact with computers/machines as tactile switch/interface,³² *etc.*

Received: November 2, 2020

Accepted: December 31, 2020

Published: January 11, 2021



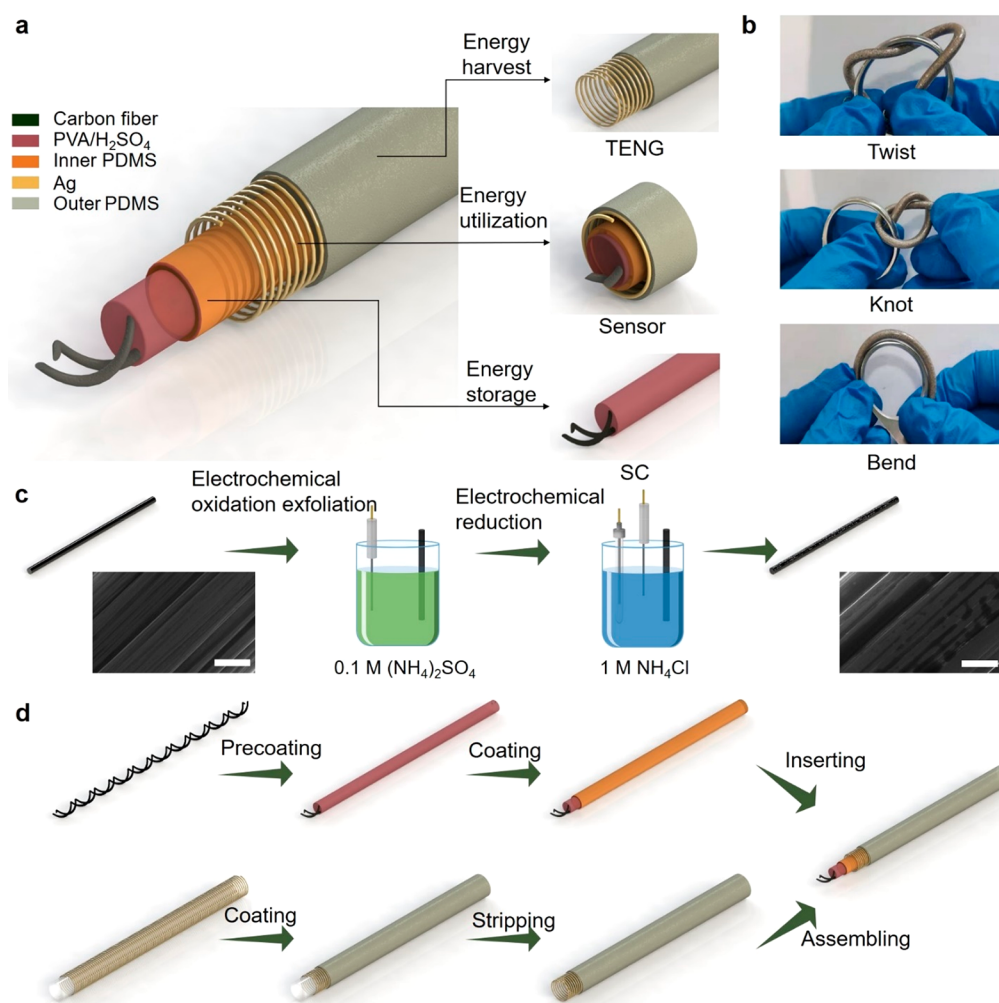


Figure 1. Schematic illustration of the energy fiber and fabrication process. (a) Schematic structure diagrams of the energy fiber for energy harvesting, storage, and utilization (including TENG, sensor, and SC). (b) Photographs of the energy fiber subjected to different mechanical deformations, including twisting, knotting, and bending. Fabrication process of (c) fibrous SC and (d) energy fiber. Insets in (c): SEM images of the carbon fiber surface morphology before and after electrochemical activation.

From the geometry aspect of the energy package, one-dimensional energy fibers/yarns/threads are highly promising compared with the bulky or planar counterparts due to their softness, weavability, shape-adaptivity, and air-permeability.^{33–35} For sustainable and continuous utilization in different application scenarios, fiber-shaped nanogenerators,^{36,37} energy storage devices,³⁸ and actuators/sensors^{33,39} are preferred to be integrated in one unit, i.e., versatile or multifunctional energy fibers. To achieve a more robust versatile energy fiber, the sophisticated design, facile fabrication process, and compact assembly of each component need to be urgently developed. The simple and easily scaled-up coaxial design is a good option with core–shell architecture including a fiber-shaped inner core and a tube-shaped outer shell.⁴⁰ Functional layers can be shared inside along the common axis to greatly save the required assembling space and achieve the multifunctional integrations.³⁴ The paired facile processing method to each functional fiber/tube is also required to achieve the versatile and robust energy fiber with a low cost, e.g., photolithography-free coating,⁴¹ green electrochemical depositions,⁴² and mild post-treatment conditions.⁴³ How to more effectively and sufficiently utilize various functional energy fibers is still a pendent imperative to be fulfilled.

Here, a multifunctional coaxial energy fiber has been developed toward energy harvesting, energy storage, and energy utilization. The energy fiber is composed of TENG, SC, and a pressure sensor (all in a fiber shape), which are integrated in a coaxial fashion. The inner core is a fibrous SC for energy storage with solid-state electrolyte gel uniformly surrounding two twisted carbon fibers (current collectors, modified by green activation strategy) and covered by a protective thin layer of polydimethylsiloxane (PDMS) and a Ag electrode. The outer sheath is a fibrous TENG in single-electrode mode for energy harvesting with a layer of PDMS supported by a metallic spring. Meanwhile, the outer PDMS friction layer and the inner PDMS layer (covered with Ag) constitute another coaxial fibrous TENG in contact-separation mode. The fibrous TENG can utilize the harvested electricity and correlate it with external pressure to work as a self-powered pressure sensor. We systematically investigate the electrical performances of each energy component. A two-step green electrochemical process is employed to prepare the SC electrodes with great chemical stability and microstructured surfaces to achieve a good length specific capacitance density of 13.42 mF·cm⁻¹, good charging/discharging rate capability, and excellent cycling stability (~96.6% capacitance remaining after 10 000 cycles at a current

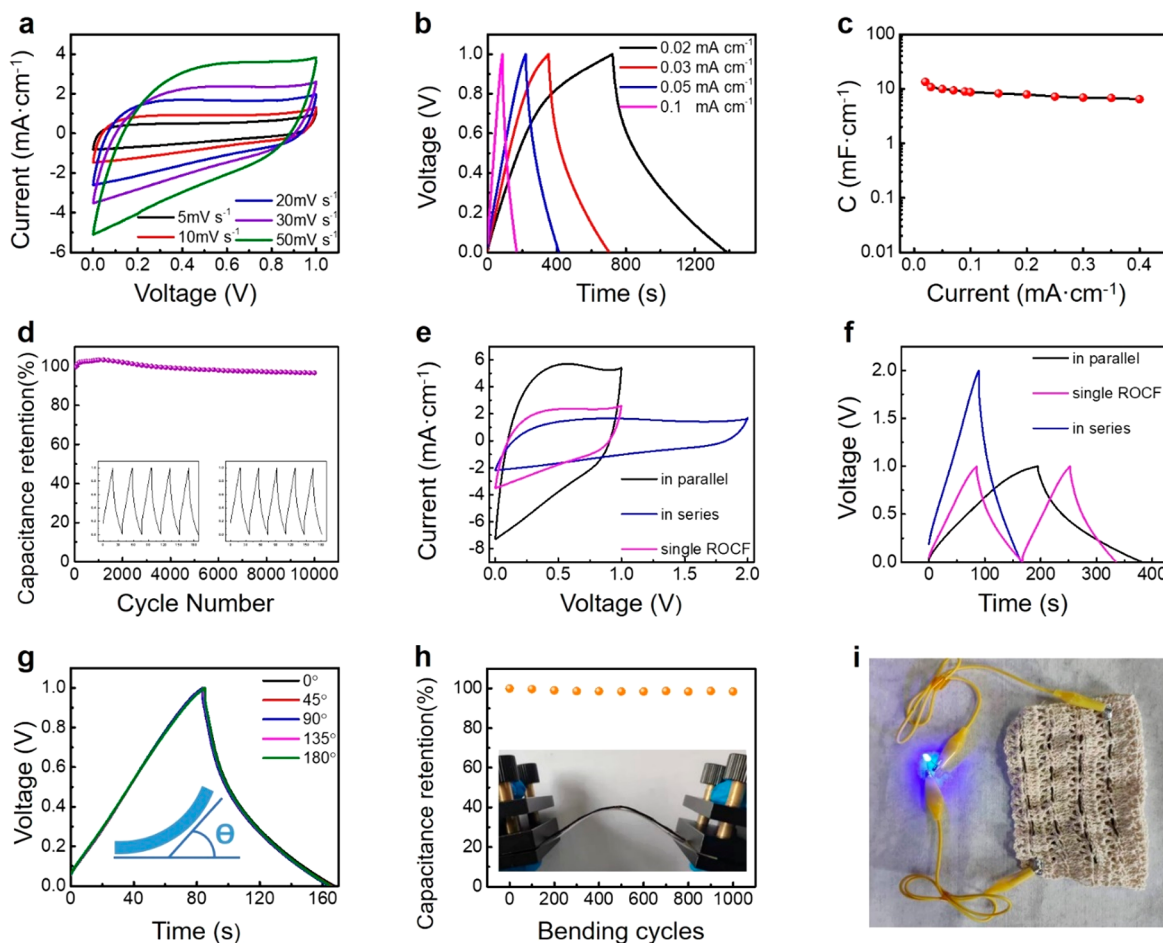


Figure 2. Electrochemical performances and flexibility of the SC. (a) Cyclic voltammetry (CV) curves obtained at different scanning rates. (b) Galvanostatic charging/discharging (GCD) plots of the SC at different current densities. (c) Variation in the specific length capacitances with discharging plots. (d) Cycling performances of the SC. (e) CV and (f) GCD curves for two SCs in parallel and in series. (g) GCD plots for the bent SC at current density of $0.1 \text{ mA}\cdot\text{cm}^{-2}$. (h) Normalized capacitances of the SC bent at 180° for 1000 cycles. (i) Photograph of a fabric woven with four fibrous SCs in series and a blue LED powered by the energy storage fabric.

density of $0.3 \text{ mA}\cdot\text{cm}^{-2}$). The fibrous TENG shows a maximum power of $2.5 \mu\text{W}$ (open circuit voltage at 10 V and short circuit current at $0.25 \mu\text{A}$) and can be used to power an electronic watch and temperature sensor. The pressure sensor has a high sensitivity of $1.003 \text{ V}\cdot\text{kPa}^{-1}$ below 23 kPa, which can readily monitor the real-time finger motions and be functionalized as a tactile interface for a fibrous electronic piano. The demonstrated multifunctional coaxial energy fiber is highly promising for wearable energy harvesting clothes, a sustainable human-machine interface, intelligent electronic skin, a smart tactile switch, *etc.*

RESULTS AND DISCUSSION

Figure 1a shows the schematic illustration of the multifunctional energy fiber in a coaxial geometry. It comprises of the fibrous TENG for energy harvesting, the SC for energy storage, and the self-powered pressure sensor by utilizing the harvested mechanical energy. The fibrous TENG is made of silver nylon yarn and elastic PDMS. It is assembled as the outer sheath, which is robust enough and ready to harvest external mechanical energy. The fibrous SC is made of activated carbon fiber and poly(vinyl alcohol)/sulfuric acid (PVA/ H_2SO_4) electrolyte. It is inserted as the inner core and covered with a protective PDMS layer. The pressure sensor is based on another TENG composed

of an outer sheath and inner core in contact-separation mode by taking advantage of the coaxial design. It can realize the self-powered sensation when the energy fiber is subjected to the external load. The assembled flexible energy fiber with a diameter of 3 mm (Figure S1) is ready to be subjected to the mechanical deformations of twisting, knotting, and bending (Figure 1b), exhibiting promising potential in wearable device applications.

As the inner core, the activated carbon fiber (CF) current collectors are first prepared prior to the fabrication of the multifunctional energy fiber, which involves a two-step electrochemical process (oxidation/exfoliation and electrochemical reduction, Figure 1c). The electrochemical exfoliation is a green and facile method where the reaction of the negative and positive ions results in the expansion of materials along the CF axis, which introduces microstructured surface morphology with additional nanogullies on the CF surface. The micro/nanostructured CF with increased surface area is beneficial for ion adsorption and can significantly enhance the energy storage capability. During the electrochemical oxidation exfoliation process, a bias voltage (+10 V) is applied between the cathode (a platinum wire) and the anode (CF) in 0.1 M ammonium sulfate ($(\text{NH}_4)_2\text{SO}_4$) aqueous solution. The applied bias induces the reduction of H_2O molecules at the cathode and introduces hydroxyl ion (OH^-) intercalation into the CF surface, which can attract active site atoms to be oxidized to functional groups (e.g.,

—C—OH, —C=O, and —COOH) and deliver enough space for the subsequent reduction process to introduce potential micro/nano-structures on the CF electrodes. The electrochemical oxidized carbon fiber with different processing times is abbreviated as EOCF-X, in which X represents the processing time. By directly using the EOCF-X samples as the working electrode, the electrochemical reduction process is carried out with three-electrode configuration in the 1.0 M NH_4Cl aqueous solution to reduce the EOCF-X samples into a reduced-oxidative carbon fiber (ROCF-X, 1 h, at a potentiostatic polarization of -1.5 V, room temperature). Due to the high diffusion efficiency of electrons in the electrolyte, electrochemical reactions between the electrons and surface oxygen-containing functional groups can be adequately implemented to achieve the ROCF-X electrodes with a square resistance of few tens of ohms. The insets of Figure 1c reveal the SEM images of the CF surface morphology before and after electrochemical activation, respectively. A rougher surface with some micro/nano-cracks is observed on the activated CF (right inset) compared with the pristine CF (left inset) due to the axial expansion of fiber materials during oxidative exfoliation. Some of the microgullies may also be originated from the accompanied evolution of gaseous species (e.g., SO_2 and O_2) during the electrochemical process. The SEM images of pristine and activated CFs with more details are shown in Figure S2.

The fabrication process for the energy fiber (assembled by the inner SC core and external TENG sheath) is shown in Figure 1d. Based on the prepared ROCF, the SC is fabricated by precoating the electrolyte with a subsequent coating of PDMS as an encapsulation layer (top panel in Figure 1d). Two strands of the ROCFs, working as the current collectors, are twisted into a spring-like spiral winding shape without contacting each other. The spiral-winding ROCFs are repeatedly immersed into PVA/ H_2SO_4 solution and casted for three times to achieve the fibrous SC. The thin layer of PDMS coated on the fibrous SC plays versatile roles as the dielectric encapsulating shell, supporting bone, and contact-electrification layer against the external sheath tube. It also shows good biocompatibility and great breathability for potential wearable applications. For the external sheath tube, a silver coated nylon yarn is first closely wound around a plastic stick and packaged by PDMS, from which the plastic stick can be drawn out with the left free-standing PDMS tube as the outer sheath (with a diameter of 2 mm, bottom panel in Figure 1d). Silver coated nylon yarn is selected as the electrode material due to its excellent electrical conductivity, mechanical robustness, and easy accessibility. To assemble the multifunctional energy fiber, the internal core column (fibrous SC with coated PDMS, with a diameter of 1 mm) is axially inserted into the external sheath tube. The coaxial geometry design can directly integrate individual functional devices and sophisticatedly synergize and share the common components to achieve the energy fiber, which is readily applicable to wearable multifunctional devices and soft electronics. Mechanical properties of the energy fiber are also evaluated by characterizing the tension versus strain properties of the fibrous TENG made of PDMS with/without silver nylon in Figure S3. The fibrous TENG made of PDMS with spiral winding silver nylon shows better mechanical properties due to that the silver nylon functionalizes as an inner supporting electrode, reinforces the mechanical properties of the composite, and strengthens the modulus of the energy fiber.

Different SC samples in aqueous H_2SO_4 solution are first characterized as shown in Figure S4 and Figure S5, among which

the ROCF-3 sample (electrochemical oxidation for three minutes) shows the best electrochemical performances. Accordingly, the electrochemical performances of the assembled all-solid-state fibrous SC (PVA/ H_2SO_4 as the hydrogel electrolyte, a symmetric configuration with two strands of ROCF-3min carbon fiber assembled in a spiral as current collectors) are mainly characterized. Figure 2a shows the cyclic voltammetry (CV) curves of the SC with ROCF-3 at various scan rates from 5 to $50 \text{ mV}\cdot\text{s}^{-1}$ with the potential window varying from 0 to 1 V. The CV curves represent slightly inclined quasi-rectangular shapes without any redox peaks, which are typical CV behaviors of the electrical double layer capacitor due to the surface electroadsorption of ion/proton incorporation with limited ion transport. Figure 2b shows that the galvanostatically charged/discharged (GCD) curves are in triangular-shaped profiles at current densities from 0.02 to $0.1 \text{ mA}\cdot\text{cm}^{-1}$, representing good electrochemical performance of the fibrous SCs with high Coulombic efficiency and fast charge propagation. The length specific capacitance density calculated from the discharging plots ranges from 13.43 to $6.44 \text{ mF}\cdot\text{cm}^{-1}$ under charging current densities from 0.02 to $0.4 \text{ mA}\cdot\text{cm}^{-1}$ (Figure 2c). The cycling performance of the fibrous SC can retain about 96.6% of the initial value even after 10 000 cycles (evaluated by GCD tests at a current density of $0.3 \text{ mA}\cdot\text{cm}^{-1}$, Figure 2d). The capacitance retention is slightly higher than 100% at the initial cycling stage, which may be attributed to that the gradually uniform wetting process of the electrodes by electrolyte leads to the falsely increased capacitance. For practical applications, a higher capacitance or voltage is required by simply connecting the fibrous SCs in series or in parallel. As shown in Figure 2e, the output current of two SCs in a parallel connection is doubled compared with a single device, and the voltage window can be easily widened to 2 V by connecting two SCs in series. Figure 2f demonstrates the GCD curves of one single SC and two SCs connected in parallel and in series. The voltage window of the series connected SCs goes up to 2.0 V (twice higher than that of the single device with the same charging/discharging time), indicating the capacitance is half that of a single SC. The charging/discharging time for two SCs in a parallel connection is twice longer than one SC, which thereby signifies the capacitance by two times. For wearable energy storage textiles, the flexibility and durability without affecting electrochemical performance are indispensable. As shown in Figure 2g, no obvious deteriorations during charging/discharging can be observed with the SC bent at different angles (0° – 180°), confirming its excellent bendability. Furthermore, the capacitance retention rate of the fibrous SC shows almost no variation after 1000 cycles of bending at 180° in Figure 2h. The inset shows a photo image of the bent SC fixed on the linear motor. For practical applications, four SCs connected in series are woven into common textiles and used to power a blue LED (Figure 2i). The excellent stability allows the series connections of more fibrous SCs to drive portable electronics with higher power consumption.

For energy harvesting, the energy fiber integrates two fibrous TENGs in different working modes. One is the single-electrode mode composed of an outer sheath and nitrile gloves for energy harvesting; the other is the contact-separation mode composed of the external sheath and inner core for sensing. For the energy harvesting TENG in the single-electrode mode (i.e., the outer sheath), the working mechanism illustrated with charge transfer processes based on triboelectrification and electrostatic induction is shown in Figure 3a. We take the nitrile glove

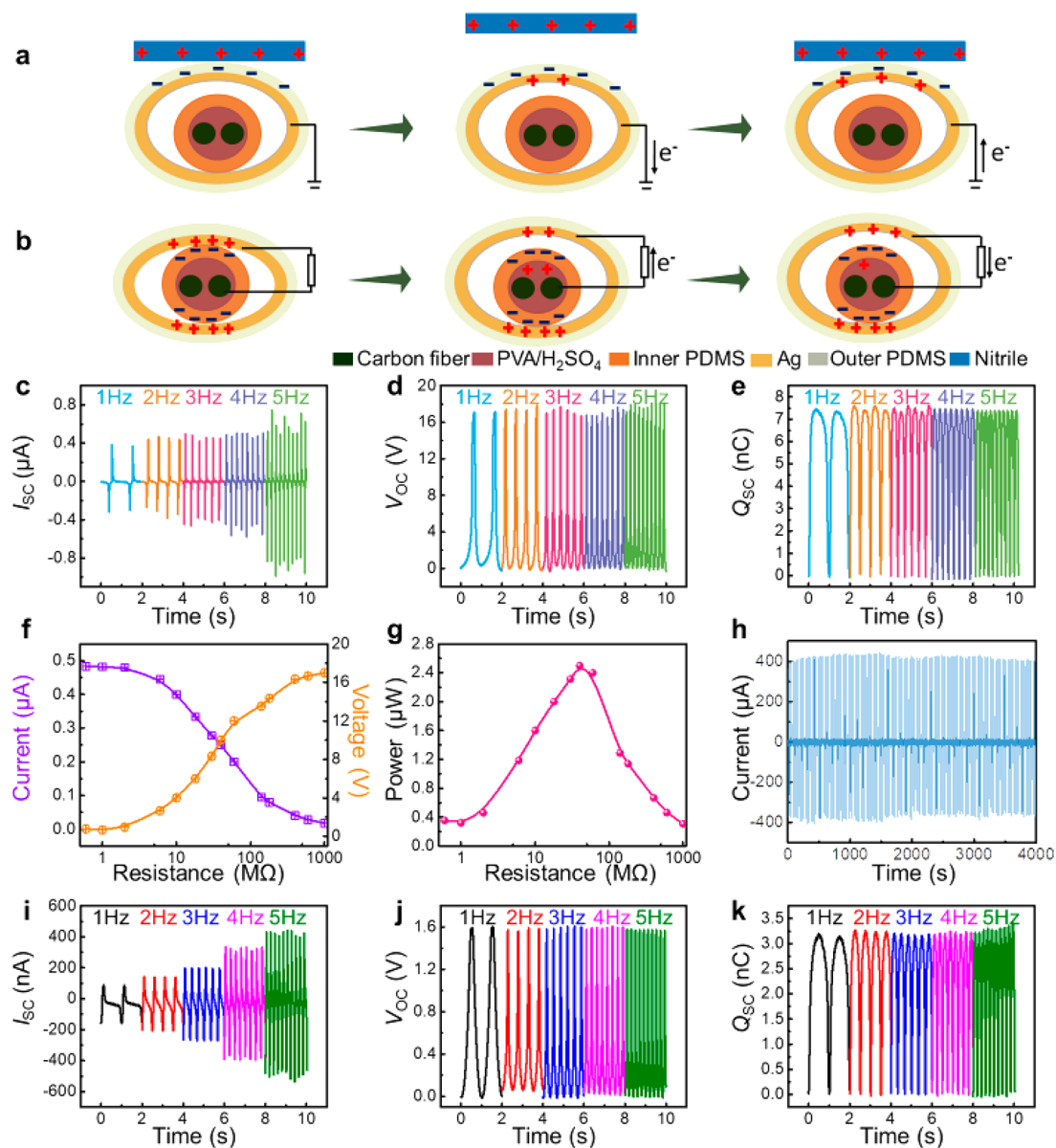


Figure 3. Working principles and electrical output performance of the energy fiber. Schematic diagram of working principles of the (a) single-electrode mode and (b) vertical contact-separation mode. Electrical outputs of the energy fiber in single-electrode mode in various compressing frequencies (1–5 Hz), which include (c) I_{sc} , (d) V_{oc} , and (e) Q_{sc} . (f) Relationship between current and voltage of the external load. (g) Instantaneous power as a function of external load resistance, calculated from the plots in (f). (h) Real-time current output of the fibrous TENG in contact-separation mode of TENG, monitored for 4000 s. Electrical outputs of the energy fiber in contact-separation mode at various compressing frequencies (1–5 Hz), which include (i) I_{sc} , (j) V_{oc} , and (k) Q_{sc} .

contacting with the single-electrode mode TENG as the example. When the surface of the glove and the outer PDMS are brought into contact with each other, surface charge transfer takes place at the contact interface due to triboelectrification. There is no electrical potential difference between the contacted glove and PDMS, thereby exhibiting no electricity between the ground and the Ag electrode. According to the triboelectric series, the nitrile glove carries positive charges on its bottom surface, inducing equivalent negative charges on the outer PDMS of the energy fiber. Due to the intrinsically insulating property of the glove and outer PDMS, the induced electrostatic charges with opposite signs can be confined on the surface for a long time. When the glove starts to separate from the outer PDMS, positive charges will be induced on the Ag electrode. The electrons from the Ag electrode are forced to flow toward

the ground due to the induced electrical potential difference between the electrode and the ground, resulting in an electrical current. Once the glove is approaching the outer PDMS again, the reduction of the distance will make the glove possess a higher electric potential than the Ag electrode, and electrons are driven from the ground back to the Ag electrode, resulting in a reversed output current signal. For the sensing TENG in contact-separation mode, the working mechanism is shown in Figure 3b, which is similar to the single-electrode mode. The only difference is that the electrons transfer between the Ag electrode and the ground in single-electrode mode, while it occurs between the Ag electrode and CFs in contact-separation mode.

The output performances of the fibrous TENG in the single-electrode mode driven by a linear motor are taken as an example and evaluated by an electrostatic meter (Keithley 6514),

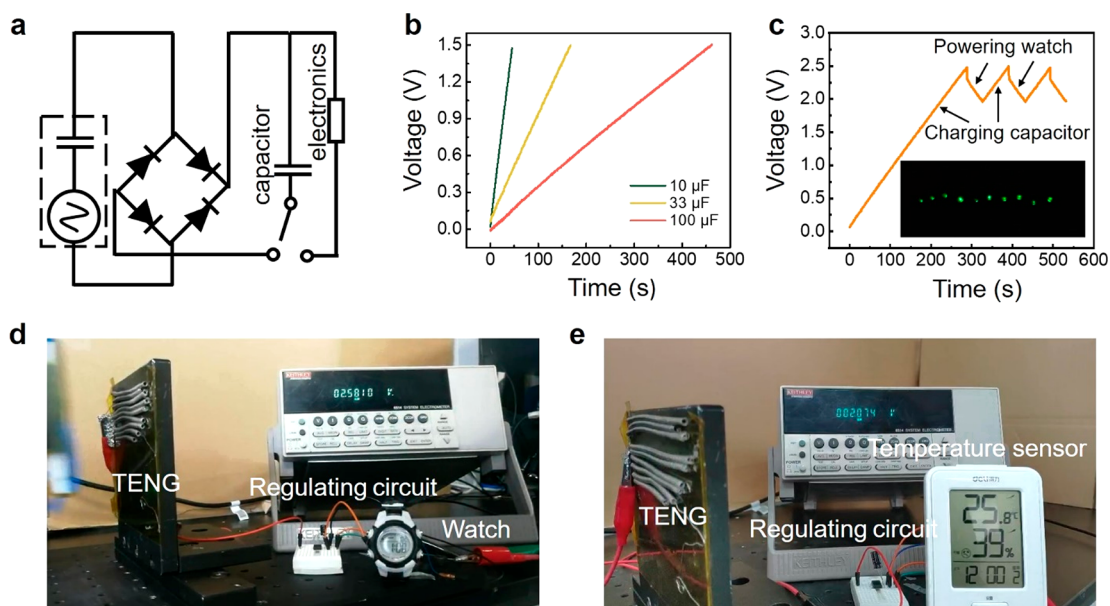


Figure 4. Energy harvesting application of the energy fiber in single-electrode mode. (a) Equivalent electrical circuit diagram for charging the energy fiber under periodic mechanical actions. (b) Charging curves of the different commercial capacitors by mechanically pressing the energy fibers. (c) Real-time test of the capacitor voltage during charging of the capacitor and periodically powering an electronic watch. Inset is 10 series-connected LEDs driven by the energy fibers. (d) Electronic watch and (e) a temperature–humidity meter driven by 9 parallel energy fibers.

including open-circuit voltage (V_{OC}), short-circuit current (I_{SC}), and transferred charges (Q_{SC}). With the contact frequency increased from 1 to 5 Hz (the contact-separation distance is at 80 mm), I_{SC} increases from 0.37 to 0.63 μA (Figure 3c), while V_{OC} and Q_{SC} almost remain constant (16.6 V and 7.3 nC in Figure 3d,e, respectively). The typical TENG output variations related to the frequency can be explained as follows. According to the Gauss theorem,⁴⁴ the voltage between the two electrodes can be given by

$$V = -\frac{Q}{S\epsilon_0} \left(\frac{d}{\epsilon} + x(t) \right) + \frac{\sigma x(t)}{\epsilon_0}$$

where Q is the amount of transferred charge and x is the separation distance between the two triboelectric charged layers. d , S , and ϵ are the thickness, electrode area, and relative dielectric constant of the PDMS, respectively. ϵ_0 is the permittivity of the vacuum. The voltage is the function of $x(t)$ and the static charge density of σ , which shows no response to the frequency. For the short-circuit current, it can be extracted from the evaluation of Maxwell's displacement current⁴⁵ in the follow equation:

$$J_D = \sigma_T \frac{dH}{dt} \frac{d\epsilon_0/\epsilon}{\left[\frac{d\epsilon_0}{\epsilon} + z \right]^2} + \frac{d\sigma_T}{dt} \frac{H}{\frac{d\epsilon_0}{\epsilon} + z}$$

where H is a function of time and it is determined by the rate at which the Ag electrode and outer PDMS are contacted. This equation means that the displacement current density (which also determines the output current) is proportional to the charge density on the static charge density of σ and the speed at which the two dielectrics contact/separate.

Various resistors are connected as external loads to further investigate the effective electrical power for driving portable electronics. As demonstrated in Figure 3f, the output current drops with the increased external load resistance due to Ohmic law, while the voltage shows a reverse trend. Accordingly, the

instantaneous power output ($W = I_{\text{peak}}^2 \cdot R$) reaches the maximum value of 2.5 μW at an external load resistance of 40 $\text{M}\Omega$. As the stability of the fibrous TENG output current is critical for ensuring a continuous power supply to portable electronics, the real-time I_{SC} of the single-electrode mode TENG is monitored at 3 Hz for 4000 s (Figure 3h). It shows relatively stable output with very slight fluctuation, guaranteeing the practical energy scavenging and sensing application of the energy fiber. We have also characterized the influence of the outer PDMS thickness on the electric output of the single-electrode mode fibrous TENG (Figure S6), among which the outer PDMS with a thickness of 0.5 mm shows the highest output. The electric performances (I_{SC} , V_{OC} , and Q_{SC}) of the other contact-separation mode fibrous TENG (Figure 3b) is also evaluated, which shows a similar variation trend with the single-electrode mode under different contact-separation frequencies (Figure 3i–k). However, the electric performance is lower (at 5 Hz, $I_{SC} = 0.4 \mu\text{A}$, $V_{OC} = 1.6 \text{ V}$, and $Q_{SC} = 3.2 \text{ nC}$) due to the finite contact area of the inner fibrous structure. The contact-separation mode fibrous TENG with relatively lower output can be considered to work as a strain sensor (which will be discussed later).

As the TENG in single-electrode mode shows higher output performance, it can be readily used as a power source. To drive commercial portable electronics, the intrinsic pulse electric output of the TENG needs to be first stored in energy storage elements such as batteries or capacitors for the subsequent supply of energy. Figure 4a shows the equivalent electrical circuit diagram. The fibrous TENG is integrated with a capacitor to form a self-charging power system, including TENG as an AC power source, a bridge rectifier as an AC-to-DC converter, and a capacitor as the energy storage device. The switch can successfully control the energy stored in the capacitor or power the series connected electronics on demand. The charging curves for 10, 33, and 100 μF capacitors by the fibrous TENG are shown in Figure 4b. It takes 45, 167, and 461 s to

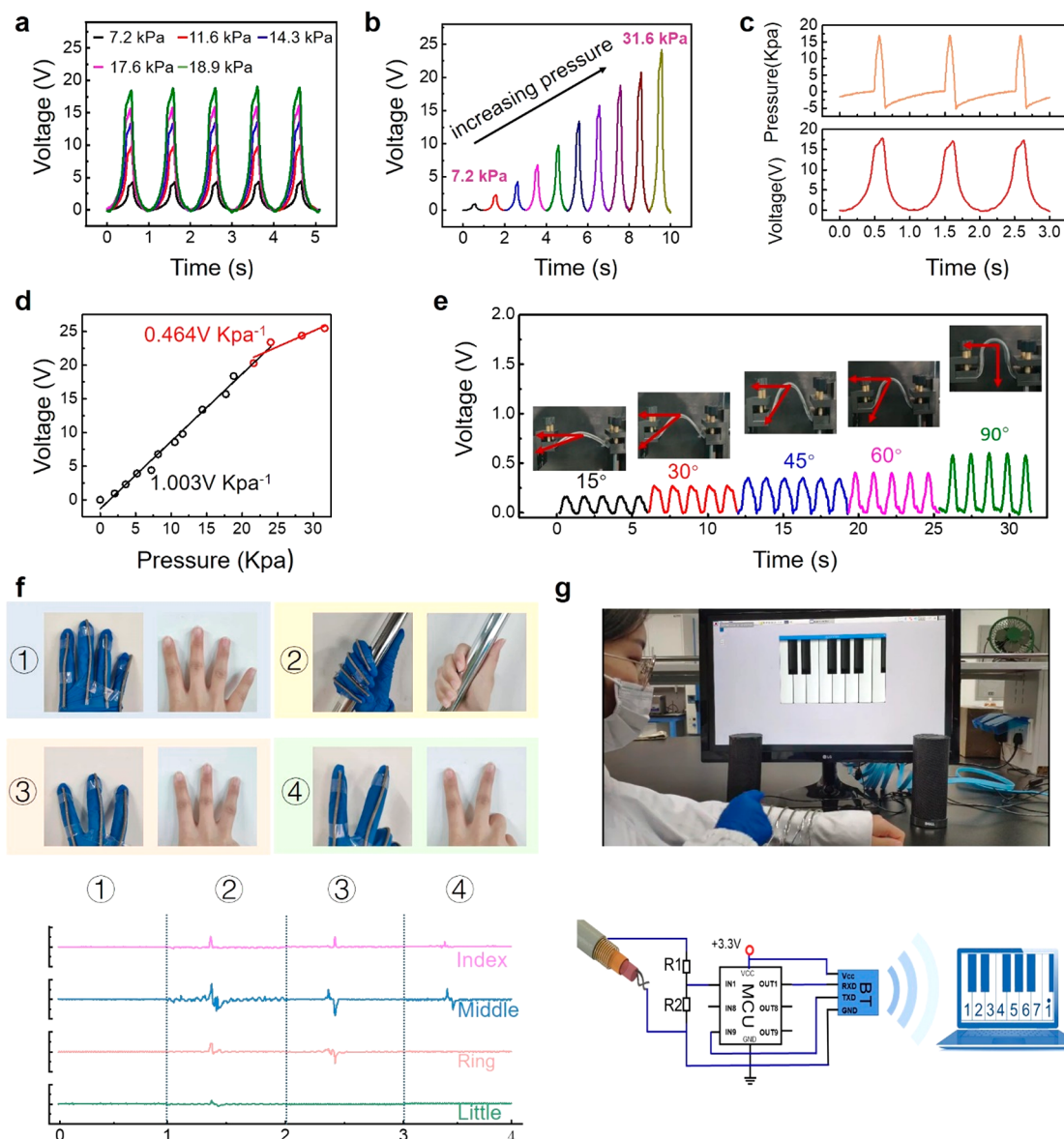


Figure 5. Pressure sensing applications of the energy fiber in single-electrode mode and contact-separation mode. (a) Static voltage response of the energy fiber under different pressures. (b) Dynamic instantaneous voltage response according to the increased pressure. (c) Real-time voltage response to applied pressure, monitored by the voltmeter and pressure gauge simultaneously. (d) Force–voltage curve of the energy fiber. (e) Output voltage of the energy fiber under different bending angles. Inset: bending energy fiber at different angles by a linear motor. (f) Photographs of a glove with four strain sensors mounted on four fingers and the corresponding hand gestures (top panel); real-time voltage sensing signals under different gestures (bottom panel). (g) Photograph of the energy fiber as the tactile interface for playing an electronic piano (top panel); circuit diagram of the fibrous tactile interface and processing circuit (bottom panel).

charge the capacitor of 10, 33, and 100 μF to 1.5 V, respectively. After completing the first charging cycle for the capacitor of 33 μF to 1.95 V in 326 s, the fibrous TENG is able to recharge the capacitor to 2.5 V in 25 s and then power the watch repeatedly (Figure 4c). Figure 4d and Movie S1 show the powering of the electronic watch (DFYJ.CO NT-62, 0.12 mW) by using nine fibrous TENGs connected in series with a 10 μF capacitor. To power a temperature–humidity meter (BLX346, 0.15 mW, 3.6 V), the fibrous TENGs are required to charge a larger capacitor (100 μF , charging plot in Figure S7) and then realize the powering process, as shown in Figure 4e and Movie S2. The fibrous TENGs can also directly light up 10 LEDs as a sustainable power source (inset of Figure 4c). In the fibrous TENG, the adopted silver thread is well packaged with PDMS, and it is lightweight, anticorrosive, and soft, which can better suit

the practical needs compared with traditional power sources based on solid materials like metal.

In addition to serving as the power source, the electrical output of the TENG is also proportional to the applied force or strain, which can be used for self-powered mechanosensation. The outer surface of the energy fiber can be directly contacted with an external object or skin (in different electronegativities) in single-electrode working mode, which allows a self-powered sensor or direct-contact interactive interface. The open-circuit voltage is utilized as the sensing signal to detect the magnitude of the pressure, which reflects the static force information applied to the fibrous TENG. Figure 5a shows a measurement of the output voltage response to the different applied forces. The magnitude of the output signal is enlarged with the applied pressure increased from 7.2 to 18.9 kPa. Five cycles of the

applied force also lead to stable output magnitudes under the imposition of each pressure value. The real-time V_{oc} sensing signals according to the applied different pressures are also recorded in Figure 5b, which steadily increase from 4.27 to 24.18 V with the pressure increased from 7.2 to 31.6 kPa. The increased V_{oc} can be attributed to that the applied increased pressure leads to the fiber expansion with an enlarged deformation magnitude, which increases the contact area and corresponding fibrous TENG output to produce a synchronous instantaneous response. Figure 5c illustrates the transient response of the pressure sensing signals along with the applied pressure; the response time is estimated to be less than 50 ms for both applying and releasing the force. The pressure sensitivity (defined as a ratio between voltage variation and applied pressure, i.e., $\Delta V/P$) is evaluated in Figure 5d, which can be divided into two typical sensory regions (a highly sensitive region below 23 kPa with a sensitivity of $1.003 \text{ V}\cdot\text{kPa}^{-1}$ and a relatively lower sensitive region beyond 23 kPa with a sensitivity of $0.464 \text{ V}\cdot\text{kPa}^{-1}$). The two-stage sensitivity, which is closely related with the transferred charges during contact electrification, is determined by the contact-compression process between the external object and the elastic fibrous pressure sensor. The initial contact stage upon smaller pressure ($<23 \text{ kPa}$) will lead to relatively larger deformation of the fibrous sensor, while the subsequent compression process with higher pressure ($>23 \text{ kPa}$) will lead to relatively smaller deformation due to that the deformation space of the fibrous TENG sensor is decreased at higher pressure region. The achieved sensitivity in the first stage is comparable to the TENG based on liquid filled tube ($1.019 \text{ V}\cdot\text{kPa}^{-1}$)⁴⁶ and much higher than the counterparts with silicone rubber coated stainless-steel thread (sensing range limited within 6 N).⁴⁷ A detailed comparison between this work and several related reports is listed in Table S1.

The fibrous TENG in contact-separation mode composed of the CF electrode, encapsulation layer of the SC (i.e., inner PDMS), and wound Ag yarns can be utilized as a strain sensor due to the effective contact-separation process induced by the applied external strain. Enlarged applied strain will lead to more contact areas between the inner PDMS and wound Ag yarns, which can result in the proportionally increased output sensing signals. When the energy fiber is repeatedly bent and relaxed (Figure 5e), the real-time V_{oc} shows a gradually and periodically synchronous increment/decrement due to the electron transfer between the Ag yarns and the CF electrode. It is obvious that the electrical outputs of the energy fiber increase from 0.16 to 0.59 V with the bending angles increased from 15° to 90° , demonstrating the potential applications of self-powered real-time motion detection. As a proof of concept, the energy fibers in contact-separation mode have been used as self-powered smart gesture-recognizing devices on a glove thanks to the sensitivity and desirable stability of periodic vibration. Four energy fibers are fixed on the dorsal side of fingers on nitrile gloves. When a hand wearing this glove makes different gestures, such as keeping all fingers straight or holding a steel bar with the four fingers (top panel of Figure 5f), the real-time voltage signals are monitored. Based on the self-powered strain sensors, instantaneous finger actions can be reflected and distinguishable by the output information on the energy fiber (bottom panel of Figure 5f). Furthermore, the energy fiber can functionalize as a tactile interface for a fibrous electronic piano, in which the triboelectric output induced by the touch between fingers and fibers can be captured by the microcontrol system and recognized to trigger the embedded software program to play the basic notes and

music (Figure 5g and Movie S3). The multifunctional applications of the energy fiber are of great significance to sustainable and adaptive wearable devices.

CONCLUSION

In summary, a multifunctional coaxial energy fiber has been developed based on fiber-shaped TENG, SC, and a pressure sensor in a coaxial design. The fibrous TENG can utilize the harvested electricity and correlate it with external pressure to work as a self-powered pressure sensor. The prepared fibrous SC achieves a good specific length capacitance density of $13.42 \text{ mF}\cdot\text{cm}^{-1}$, good charging/discharging rate capability, and excellent cycling stability. The fibrous TENG shows a maximum power of $2.5 \mu\text{W}$ and can be used to power an electronic watch and temperature sensor. The self-powered pressure sensor shows a sensitivity of $1.003 \text{ V}\cdot\text{kPa}^{-1}$ and can be readily used to monitor the real-time finger motions and work as a tactile interface. The demonstrated versatile and compact coaxial energy fibers will lead the textile wearable electronics toward a more intelligent, more accessible, and more environmentally friendly development direction.

METHODS

Electrochemical Activation of Carbon Fiber. The carbon fiber was prepared by electrochemical oxidative treatment followed by electrochemical reduction. Before activation, a strand of carbon fibers was rinsed in deionized (DI) water several times and dried in a vacuum oven. The electrochemical oxidative treatment was implemented in a standard two-electrode configuration that was constructed with a platinum plate electrode as the cathode and a strand of carbon fibers as the anode in 70 mL of 0.1 M $(\text{NH}_4)_2\text{SO}_4$ aqueous solution. A direct current voltage of +10 V was applied between the two electrodes with the processing times of 1, 2, 3, and 5 min for each sample, respectively. The electrochemical reduction was carried out in a three-electrode system with 50 mL of 1.0 M NH_4Cl aqueous solution as the electrolyte, in which a platinum plate electrode was employed as the counter electrode, an Ag/AgCl electrode worked as the reference electrode, and the oxidative carbon fiber was directly used as the working electrode. All these electrodes were reduced under potentiostatic polarization at -1.5 V for 1 h at room temperature. Then the ROCFs were washed with DI water and dried in a vacuum oven for the following experiments.

Fabrication of the Supercapacitor Electrode. The PVA gel solution was first prepared by dissolving 5 g of PVA ($M_w = 89\,000\text{--}98\,000$) in 20 mL of DI water, heated to 90°C , and stirred for 1 h. Afterward, 5 mL of diluted H_2SO_4 in 30 mL of DI water was slowly dropped in PVA gel solution and cooled down to 20°C after uniform mixing. Electrochemical oxidation and reduction treated carbon fiber was immersed into the PVA/ H_2SO_4 hydrogel electrolyte for 1 min to coat the electrolyte gel, and then the carbon fiber was located into a vacuum oven for 15 min to remove the water. The coating and heating processes were repeated in turn for several times. The other carbon fiber was also prepared following the above methods. Then the two strands of carbon fibers were twisted into a spiral shape to assemble the fibrous SC, which was finally encapsulated by PDMS.

Characterization and Electrochemical Measurements of the SC Fiber. The surface morphologies of the carbon fiber before and after electrochemical activation were performed by a field emission scanning electron microscope (SU-8020, Hitachi). The electrochemical properties of the SC fiber were investigated by an electrochemical workstation (CHI760E Instruments, China). The specific length capacitances (C_L) with the units of $\text{F}\cdot\text{cm}^{-1}$ were calculated from galvanostatic charging/discharging plots and derived according to the following equation:

$$C_L = \frac{I \cdot \Delta t}{\Delta V \cdot L}$$

where I is the discharging current, Δt is the discharging time, ΔV is the voltage difference in consideration of the current-resistance drop, and L is the length of the carbon fiber.

Fabrication of the Energy Fiber. For the systematic design of the energy fiber, commercial silver-coated nylon yarn (nominal diameter: 270 μm , resistance $< 5 \Omega \cdot \text{cm}^{-1}$) was selected as the outer electrode, and PDMS (Sylgard 184, Dow Corning) was chosen as the dielectric, supporting, and encapsulating material. First, PDMS as a dielectric material was prepared by mixing the base monomers and the curing agent with the ratio of 10:1 by weight. After mixing, the solution of PDMS was degassed in a vacuum oven at room temperature for 30 min to thoroughly remove the bubbles. Second, the plastic stick (diameter: 2 mm) was spirally wound by a silver-coated nylon yarn (outer electrode) along its axial direction and then put into another plastic tube mold (diameter: 3 mm). Third, the solution of the prepared PDMS was syringed into the mold along the tube wall to slowly fill the tube, and then the tube was put in an oven for overnight at 80 $^{\circ}\text{C}$ to thermally solidify the PDMS. Thus, the PDMS-encapsulated spiral silver-coated nylon sheath TENG (thickness: 0.5 mm) could be obtained by peeling off the outer plastic tube and pulling out the inner plastic stick.

Characterization of the Energy Fiber. To characterize the output measurement of the energy fiber, the contact-separation action was applied by a commercial linear mechanical motor. V_{OC} , I_{SC} , and Q_{SC} were measured by an electrometer (Keithley 6541 system). A custom LabVIEW program was used to record the electrical output. A force detector (YMC 501F01, 8 mm diameter) was used to sense the applied force. The external force was also applied by the linear mechanical motor, and the real-time pressure sensing based on the output of the energy fiber was measured by an oscilloscope. The diameter of the PDMS-coated outer sheath and SC fiber were measured by an electronic digital micrometer (733 Series Electronic Digital Micrometers, L. S. Starrett).

ASSOCIATED CONTENT

Supporting Information

The Supporting Information is available free of charge at <https://pubs.acs.org/doi/10.1021/acsnano.0c09146>.

Diameter dimension photograph of the energy fiber; SEM images of untreated filaments in carbon fiber and electrochemical activated filaments in carbon fiber; tension vs strain properties of the fibrous TENG made of PDMS with/without silver nylon; electrochemical performances of the CF and ROCF-X; electrochemical performances of the OCF and ROCF-3 min; electrical output performance of the fibrous TENG with different thicknesses of outer PDMS; charging curve of the 100 μF commercial capacitor charged by mechanically pressing energy fibers; and detailed comparison between this work and several related reports (refs 37, 46, and 47) (PDF)

Powering an electronic watch by energy fibers (MP4)

Powering a wireless temperature/humidity sensor by energy fibers (MP4)

Energy fiber as a tactile switch for an electronic piano (MP4)

AUTHOR INFORMATION

Corresponding Authors

Qijun Sun – Beijing Institute of Nanoenergy and Nanosystems, Chinese Academy of Sciences, Beijing 101400, P. R. China; School of Nanoscience and Technology, University of Chinese Academy of Sciences, Beijing 100049, P. R. China; Center on Nanoenergy Research, School of Physical Science and Technology, Guangxi University, Nanning 530004, P. R.

China; orcid.org/0000-0003-2130-7389;

Email: sunqijun@binn.cas.cn

Junyi Zhai – Beijing Institute of Nanoenergy and Nanosystems, Chinese Academy of Sciences, Beijing 101400, P. R. China; School of Nanoscience and Technology, University of Chinese Academy of Sciences, Beijing 100049, P. R. China; Center on Nanoenergy Research, School of Physical Science and Technology, Guangxi University, Nanning 530004, P. R. China; orcid.org/0000-0001-8900-4638; Email: jyzhai@binn.cas.cn

Zhong Lin Wang – Beijing Institute of Nanoenergy and Nanosystems, Chinese Academy of Sciences, Beijing 101400, P. R. China; School of Nanoscience and Technology, University of Chinese Academy of Sciences, Beijing 100049, P. R. China; School of Materials Science and Engineering, Georgia Institute of Technology, Atlanta, Georgia 30332-0245, United States; orcid.org/0000-0002-5530-0380; Email: zhong.wang@mse.gatech.edu

Authors

Jing Han – Beijing Institute of Nanoenergy and Nanosystems, Chinese Academy of Sciences, Beijing 101400, P. R. China; School of Nanoscience and Technology, University of Chinese Academy of Sciences, Beijing 100049, P. R. China

Chongyang Xu – Beijing Institute of Nanoenergy and Nanosystems, Chinese Academy of Sciences, Beijing 101400, P. R. China

Jintao Zhang – Beijing Institute of Nanoenergy and Nanosystems, Chinese Academy of Sciences, Beijing 101400, P. R. China; School of Mathematics and Physics, Shanghai Key Laboratory of Materials Protection and Advanced Materials in Electric Power, Shanghai University of Electric Power, Shanghai 200090, P. R. China

Nuo Xu – Beijing Institute of Nanoenergy and Nanosystems, Chinese Academy of Sciences, Beijing 101400, P. R. China; Center on Nanoenergy Research, School of Physical Science and Technology, Guangxi University, Nanning 530004, P. R. China

Yao Xiong – Beijing Institute of Nanoenergy and Nanosystems, Chinese Academy of Sciences, Beijing 101400, P. R. China; School of Nanoscience and Technology, University of Chinese Academy of Sciences, Beijing 100049, P. R. China

Xiaole Cao – Beijing Institute of Nanoenergy and Nanosystems, Chinese Academy of Sciences, Beijing 101400, P. R. China; School of Nanoscience and Technology, University of Chinese Academy of Sciences, Beijing 100049, P. R. China

Yuchen Liang – Beijing Institute of Nanoenergy and Nanosystems, Chinese Academy of Sciences, Beijing 101400, P. R. China; Qichen (Shanghai) Medical Co., Ltd., Shanghai 201319, P. R. China

Li Zheng – School of Mathematics and Physics, Shanghai Key Laboratory of Materials Protection and Advanced Materials in Electric Power, Shanghai University of Electric Power, Shanghai 200090, P. R. China

Jia Sun – School of Physics and Electronics, Central South University, Changsha 410083, China; orcid.org/0000-0003-4423-8128

Complete contact information is available at: <https://pubs.acs.org/doi/10.1021/acsnano.0c09146>

Author Contributions

[▽](J.H. and C.X.) These authors contributed equally.

Notes

The authors declare no competing financial interest.

ACKNOWLEDGMENTS

This work is financially supported by the National Key Research and Development Program of China (2016YFA0202703), the National Natural Science Foundation of China (52073031, 51605034, 51711540300), the Fundamental Research Funds for the Central Universities (E0EG6801X2), Beijing Nova Program (Z191100001119047), the “Hundred Talents Program” of the Chinese Academy of Science.

REFERENCES

- (1) Mackanic, D. G.; Chang, T. H.; Huang, Z.; Cui, Y.; Bao, Z. Stretchable Electrochemical Energy Storage Devices. *Chem. Soc. Rev.* **2020**, *49* (13), 4466–4495.
- (2) Peng, H. Fiber Electronics. *Adv. Mater.* **2020**, *32* (5), 1904697.
- (3) Gao, G.; Yu, J.; Yang, X.; Pang, Y.; Zhao, J.; Pan, C.; Sun, Q.; Wang, Z. L. Triboiontronic Transistor of MoS₂. *Adv. Mater.* **2019**, *31* (7), No. 1806905.
- (4) Yang, X.; Han, J.; Yu, J.; Chen, Y.; Zhang, H.; Ding, M.; Jia, C.; Sun, J.; Sun, Q.; Wang, Z. L. Versatile Triboiontronic Transistor via Proton Conductor. *ACS Nano* **2020**, *14* (7), 8668–8677.
- (5) Park, S.; Heo, S. W.; Lee, W.; Inoue, D.; Jiang, Z.; Yu, K.; Jinno, H.; Hashizume, D.; Sekino, M.; Yokota, T.; Fukuda, K.; Tajima, K.; Someya, T. Self-Powered Ultra-Flexible Electronics via Nano-Grating-Patterned Organic Photovoltaics. *Nature* **2018**, *561* (7724), 516–521.
- (6) Dong, K.; Deng, J.; Zi, Y.; Wang, Y. C.; Xu, C.; Zou, H.; Ding, W.; Dai, Y.; Gu, B.; Sun, B.; Wang, Z. L. 3D Orthogonal Woven Triboelectric Nanogenerator for Effective Biomechanical Energy Harvesting and as Self-Powered Active Motion Sensors. *Adv. Mater.* **2017**, *29* (38), 1702648.
- (7) Yang, H. M.; Deng, M. M.; Tang, Q.; He, W. C.; Hu, C. G.; Xi, Y.; Liu, R. C.; Wang, Z. L. A Nonencapsulative Pendulum-Like Paper-Based Hybrid Nanogenerator for Energy Harvesting. *Adv. Energy Mater.* **2019**, *9* (33), 1901149.
- (8) He, X.; Zi, Y. L.; Guo, H. Y.; Zheng, H. W.; Xi, Y.; Wu, C. S.; Wang, J.; Zhang, W.; Lu, C. H.; Wang, Z. L. A Highly Stretchable Fiber-Based Triboelectric Nanogenerator for Self-Powered Wearable Electronics. *Adv. Funct. Mater.* **2017**, *27* (4), 1604378.
- (9) Yang, J.; Yang, F.; Zhao, L.; Shang, W.; Qin, H.; Wang, S.; Jiang, X.; Cheng, G.; Du, Z. Managing and Optimizing the Output Performances of a Triboelectric Nanogenerator by a Self-Powered Electrostatic Vibrator Switch. *Nano Energy* **2018**, *46*, 220–228.
- (10) Sun, H.; Zhu, G.; Xu, X.; Liao, M.; Li, Y. Y.; Angell, M.; Gu, M.; Zhu, Y.; Hung, W. H.; Li, J.; Kuang, Y.; Meng, Y.; Lin, M. C.; Peng, H.; Dai, H. A Safe and Non-Flammable Sodium Metal Battery Based on An Ionic Liquid Electrolyte. *Nat. Commun.* **2019**, *10* (1), 3302.
- (11) Fan, F. R.; Lin, L.; Zhu, G.; Wu, W.; Zhang, R.; Wang, Z. L. Transparent Triboelectric Nanogenerators and Self-Powered Pressure Sensors Based on Micropatterned Plastic Films. *Nano Lett.* **2012**, *12* (6), 3109–3114.
- (12) Sun, Q.; Ho, D. H.; Choi, Y.; Pan, C.; Kim, D. H.; Wang, Z. L.; Cho, J. H. Piezopotential-Programmed Multilevel Nonvolatile Memory As Triggered by Mechanical Stimuli. *ACS Nano* **2016**, *10* (12), 11037–11043.
- (13) Qin, S. S.; Zhang, Q.; Yang, X. X.; Liu, M. M.; Sun, Q. J.; Wang, Z. L. Hybrid Piezo/Triboelectric-Driven Self-Charging Electrochromic Supercapacitor Power Package. *Adv. Energy Mater.* **2018**, *8* (23), 1800069.
- (14) Zhao, C. L.; Zhang, Q.; Zhang, W. L.; Du, X. Y.; Zhang, Y.; Gong, S. B.; Ren, K. L.; Sun, Q. J.; Wang, Z. L. Hybrid Piezo/Triboelectric Nanogenerator for Highly Efficient and Stable Rotation Energy Harvesting. *Nano Energy* **2019**, *57*, 440–449.
- (15) Cheng, X. L.; Miao, L. M.; Song, Y.; Su, Z. M.; Chen, H. T.; Chen, X. X.; Zhang, J. X.; Zhang, H. X. High Efficiency Power Management and Charge Boosting Strategy for a Triboelectric Nanogenerator. *Nano Energy* **2017**, *38*, 438–456.
- (16) Xi, F. B.; Pang, Y. K.; Li, W.; Jiang, T.; Zhang, L. M.; Guo, T.; Liu, G. X.; Zhang, C.; Wang, Z. L. Universal Power Management Strategy for Triboelectric Nanogenerator. *Nano Energy* **2017**, *37*, 168–176.
- (17) Zi, Y.; Niu, S.; Wang, J.; Wen, Z.; Tang, W.; Wang, Z. L. Standards and Figure-of-Merits for Quantifying the Performance of Triboelectric Nanogenerators. *Nat. Commun.* **2015**, *6*, 8376.
- (18) Zhang, Z.; Jiang, D.; Zhao, J.; Liu, G.; Bu, T.; Zhang, C.; Wang, Z. L. Tribovoltaic Effect on Metal–Semiconductor Interface for Direct-Current Low-Impedance Triboelectric Nanogenerators. *Adv. Energy Mater.* **2020**, *10* (9), 1903713.
- (19) Liu, D.; Yin, X.; Guo, H.; Zhou, L.; Li, X.; Zhang, C.; Wang, J.; Wang, Z. L. A Constant Current Triboelectric Nanogenerator Arising from Electrostatic Breakdown. *Sci. Adv.* **2019**, *5* (4), eaav6437.
- (20) Chen, C.; Guo, H.; Chen, L.; Wang, Y. C.; Pu, X.; Yu, W.; Wang, F.; Du, Z.; Wang, Z. L. Direct Current Fabric Triboelectric Nanogenerator for Biomotion Energy Harvesting. *ACS Nano* **2020**, *14* (4), 4585–4594.
- (21) Fan, F.-R.; Tian, Z.-Q.; Lin Wang, Z. Flexible Triboelectric Generator. *Nano Energy* **2012**, *1* (2), 328–334.
- (22) Zi, Y.; Guo, H.; Wen, Z.; Yeh, M. H.; Hu, C.; Wang, Z. L. Harvesting Low-Frequency (<5 Hz) Irregular Mechanical Energy: A Possible Killer Application of Triboelectric Nanogenerator. *ACS Nano* **2016**, *10* (4), 4797–4805.
- (23) Qian, C.; Sun, J.; Kong, L.-A.; Fu, Y.; Chen, Y.; Wang, J.; Wang, S.; Xie, H.; Huang, H.; Yang, J.; Gao, Y. Multilevel Nonvolatile Organic Photomemory Based on Vanadyl-Phthalocyanine/para-Sexiphenyl Heterojunctions. *ACS Photonics* **2017**, *4*, 2573–2579.
- (24) Jiang, Q.; Wu, C. S.; Wang, Z. J.; Wang, A. C.; He, J. H.; Wang, Z. L.; Alshareef, H. N. MXene Electrochemical Microsupercapacitor Integrated with Triboelectric Nanogenerator as A Wearable Self-Charging Power Unit. *Nano Energy* **2018**, *45*, 266–272.
- (25) Wang, J.; Chen, Y.; Kong, L.-A.; Fu, Y.; Gao, Y.; Sun, J. Deep-Ultraviolet-Triggered Neuromorphic Functions in In-Zn-O Phototransistors. *Appl. Phys. Lett.* **2018**, *113*, 151101.
- (26) Sun, J.; Fu, Y.; Wan, Q. Organic Synaptic Devices for Neuromorphic Systems. *J. Phys. D: Appl. Phys.* **2018**, *51*, 314004.
- (27) Pu, J.; Wang, X.; Xu, R.; Komvopoulos, K. Highly Stretchable Microsupercapacitor Arrays with Honeycomb Structures for Integrated Wearable Electronic Systems. *ACS Nano* **2016**, *10* (10), 9306–9315.
- (28) Pu, X.; Li, L.; Liu, M.; Jiang, C.; Du, C.; Zhao, Z.; Hu, W.; Wang, Z. L. Wearable Self-Charging Power Textile Based on Flexible Yarn Supercapacitors and Fabric Nanogenerators. *Adv. Mater.* **2016**, *28* (1), 98–105.
- (29) Kong, L.-A.; Sun, J.; Qian, C.; Gou, G.; He, Y.; Yang, J.; Gao, Y. Ion-Gel Gated Field-Effect Transistors with Solution-Processed Oxide Semiconductors for Bioinspired Artificial Synapses. *Org. Electron.* **2016**, *39*, 64–70.
- (30) Yang, Y.; Han, J.; Huang, J.; Sun, J.; Wang, Z. L.; Seo, S.; Sun, Q. Stretchable Energy-Harvesting Tactile Interactive Interface with Liquid-Metal-Nanoparticle-Based Electrodes. *Adv. Funct. Mater.* **2020**, *30* (29), 1909652.
- (31) Ho, D. H.; Han, J.; Huang, J.; Choi, Y. Y.; Cheon, S.; Sun, J.; Lei, Y.; Park, G. S.; Wang, Z. L.; Sun, Q.; Cho, J. H. β -Phase-Preferential Blow-Spun Fabrics for Wearable Triboelectric Nanogenerators and Textile Interactive Interface. *Nano Energy* **2020**, *77*, 105262.
- (32) Huang, J. R.; Yang, X. X.; Yu, J. R.; Han, J.; Jia, C. K.; Ding, M.; Sun, J.; Cao, X. L.; Sun, Q. J.; Wang, Z. L. A Universal and Arbitrary Tactile Interactive System Based on Self-Powered Optical Communication. *Nano Energy* **2020**, *69*, 104419.
- (33) Kong, L.-A.; Sun, J.; Qian, C.; Wang, C.; Yang, J.; Gao, Y. Spatially-Correlated Neuron Transistors with Ion-Gel Gating for Brain-Inspired Applications. *Org. Electron.* **2017**, *44*, 25–31.
- (34) Dong, K.; Deng, J. A.; Ding, W. B.; Wang, A. C.; Wang, P. H.; Cheng, C. Y.; Wang, Y. C.; Jin, L. M.; Gu, B. H.; Sun, B. Z.; Wang, Z. L. Versatile Core-Sheath Yarn for Sustainable Biomechanical Energy Harvesting and Real-Time Human-Interactive Sensing. *Adv. Energy Mater.* **2018**, *8* (23), 1801114.

(35) Gong, W.; Hou, C.; Zhou, J.; Guo, Y.; Zhang, W.; Li, Y.; Zhang, Q.; Wang, H. Continuous and Scalable Manufacture of Amphibious Energy Yarns and Textiles. *Nat. Commun.* **2019**, *10* (1), 868.

(36) Wang, J.; Li, S.; Yi, F.; Zi, Y.; Lin, J.; Wang, X.; Xu, Y.; Wang, Z. L. Sustainably Powering Wearable Electronics Solely by Biomechanical Energy. *Nat. Commun.* **2016**, *7*, 12744.

(37) Dong, K.; Wang, Y. C.; Deng, J.; Dai, Y.; Zhang, S. L.; Zou, H.; Gu, B.; Sun, B.; Wang, Z. L. A Highly Stretchable and Washable All-Yarn-Based Self-Charging Knitting Power Textile Composed of Fiber Triboelectric Nanogenerators and Supercapacitors. *ACS Nano* **2017**, *11* (9), 9490–9499.

(38) Yang, Y.; Xie, L.; Wen, Z.; Chen, C.; Chen, X.; Wei, A.; Cheng, P.; Xie, X.; Sun, X. Coaxial Triboelectric Nanogenerator and Supercapacitor Fiber-Based Self-Charging Power Fabric. *ACS Appl. Mater. Interfaces* **2018**, *10* (49), 42356–42362.

(39) Dong, K.; Wu, Z.; Deng, J.; Wang, A. C.; Zou, H.; Chen, C.; Hu, D.; Gu, B.; Sun, B.; Wang, Z. L. A Stretchable Yarn Embedded Triboelectric Nanogenerator as Electronic Skin for Biomechanical Energy Harvesting and Multifunctional Pressure Sensing. *Adv. Mater.* **2018**, *30* (43), 1804944.

(40) Gong, W.; Hou, C. Y.; Guo, Y. B.; Zhou, J.; Mu, J. K.; Li, Y. G.; Zhang, Q. H.; Wang, H. Z. A Wearable, Fibroid, Self-Powered Active Kinematic Sensor Based on Stretchable Sheath-Core Structural Triboelectric Fibers. *Nano Energy* **2017**, *39*, 673–683.

(41) Sadeghi, M.; Delparastan, P.; Pierre, A.; Arias, A. C. Printed Flexible Organic Transistors with Tunable Aspect Ratios. *Adv. Electron. Mater.* **2020**, *6* (2), 1901207.

(42) Ye, D.; Yu, Y.; Tang, J.; Liu, L.; Wu, Y. Electrochemical Activation of Carbon Cloth in Aqueous Inorganic Salt Solution for Superior Capacitive Performance. *Nanoscale* **2016**, *8* (19), 10406–10414.

(43) Wang, L.; Wang, L. Y.; Zhang, Y.; Pan, J.; Li, S. Y.; Sun, X. M.; Zhang, B.; Peng, H. S. Weaving Sensing Fibers into Electrochemical Fabric for Real-Time Health Monitoring. *Adv. Funct. Mater.* **2018**, *28* (42), 1804456.

(44) Niu, S. M.; Wang, S. H.; Lin, L.; Liu, Y.; Zhou, Y. S.; Hu, Y. F.; Wang, Z. L. Theoretical Study of Contact-Mode Triboelectric Nanogenerators as An Effective Power Source. *Energy Environ. Sci.* **2013**, *6* (12), 3576–3583.

(45) Wang, Z. L. On the First Principle Theory of Nanogenerators from Maxwell's Equations. *Nano Energy* **2020**, *68*, 104272.

(46) Yuan, Z.; Du, X.; Niu, H.; Li, N.; Shen, G.; Li, C.; Wang, Z. L. Motion Recognition by A Liquid Filled Tubular Triboelectric Nanogenerator. *Nanoscale* **2019**, *11* (2), 495–503.

(47) Lai, Y. C.; Deng, J.; Zhang, S. L.; Niu, S.; Guo, H.; Wang, Z. L. Single-Thread-Based Wearable and Highly Stretchable Triboelectric Nanogenerators and Their Applications in Cloth-Based Self-Powered Human-Interactive and Biomedical Sensing. *Adv. Funct. Mater.* **2017**, *27* (1), 1604462.